OPEN ACCESS Freely available online

PLoS one

Targeting of Voltage-Gated Calcium Channel $\alpha_2\delta$-1 Subunit to Lipid Rafts Is Independent from a GPI-Anchoring Motif

Philip Robinson, Sarah Etheridge, Lele Song, Riddhi Shah, Elizabeth M. Fitzgerald*, Owen T. Jones*

Faculty of Life Sciences,University of Manchester,Core Technology Facility, Manchester, United Kingdom

Abstract

Voltage-gated calcium channels (Ca_v) exist as heteromultimers comprising a pore-forming α_1 with accessory β and $\alpha_2\delta$ subunits which modify channel trafficking and function. We previously showed that $\alpha_2\delta$-1 (and likely the other mammalian $\alpha_2\delta$ isoforms - $\alpha_2\delta$-2, 3 and 4) is required for targeting Ca_vs to lipid rafts, although the mechanism remains unclear. Whilst originally understood to have a classical type I transmembrane (TM) topology, recent evidence suggests the $\alpha_2\delta$ subunit contains a glycosylphosphatidylinositol (GPI)-anchor that mediates its association with lipid rafts. To test this notion, we have used a strategy based on the expression of chimera, where the reported GPI-anchoring sequences in the gabapentinoid-sensitive $\alpha_2\delta$-1 subunit have been substituted with those of a functionally inert Type I TM-spanning protein – PIN-G. Using imaging, electrophysiology and biochemistry, we find that lipid raft association of PIN-$\alpha_2\delta$ is unaffected by substitution of the GPI motif with the TM domain of PIN-G. Moreover, the presence of the GPI motif alone is not sufficient for raft localisation, suggesting that upstream residues are required. GPI-anchoring is susceptible to phosphatidylinositol-phospholipase C (PI-PLC) cleavage. However, whilst raft localisation of PIN-$\alpha_2\delta$ is disrupted by PI-PLC treatment, this is assay-dependent and non-specific effects of PI-PLC are observed on the distribution of the endogenous raft marker, caveolin, but not flotillin. Taken together, these data are most consistent with a model where $\alpha_2\delta$-1 retains its type I transmembrane topology and its targeting to lipid rafts is governed by sequences upstream of the putative GPI anchor, that promote protein-protein, rather than lipid-lipid interactions.

Citation: Robinson P, Etheridge S, Song L, Shah R, Fitzgerald EM, et al. (2011) Targeting of Voltage-Gated Calcium Channel $\alpha_2\delta$-1 Subunit to Lipid Rafts Is Independent from a GPI-Anchoring Motif. PLoS ONE 6(6): e19802. doi:10.1371/journal.pone.0019802

Editor: Vadim E. Degtyar, University of California, Berkeley, United States of America

Received December 21, 2010; **Accepted** April 14, 2011; **Published** June 10, 2011

Funding: This work was supported by funds from the Medical Research Council, UK (Project Grant I.D. 81568 to EF and OJ). www.mrc.ac.uk/. The funders had no role in study design, data collection and analysis, decision to publish, or preparation of the manuscript.

Competing Interests: The authors have declared that no competing interests exist.

* E-mail: Owen.t.jones@manchester.ac.uk (OTJ); Elizabeth.m.fitzgerald@manchester.ac.uk (EMF)

Introduction

Voltage-gated calcium channels (Ca_vs) represent the primary means by which changes in membrane potential are coupled to the influx of second messenger calcium ions [1]. As such, Ca_vs play a major role in orchestrating diverse excitable cell functions, ranging from rapid events such as neurotransmitter release in nerves and excitation-contraction coupling in muscle, to longer lasting events such as synaptic plasticity. While it is well established that disruption of Ca_vs is involved in diverse pathologies, including neuropathic pain [2] and cardiac arrhythmia [3], much less is known about how Ca_v functionality is modulated, physiologically, at the cellular level [4].

Biochemical and reconstitution studies show that Ca_vs comprise an α_1 subunit (≈200 kDa) containing the voltage-sensing, gating and pore machineries [1], [5]. In high voltage-activated Ca_v1 and Ca_v2 family channels, α_1 is complexed in a 1:1 stoichiometry with a cytoplasmic auxiliary β subunit. These channels are also complexed with a second auxiliary (≈125 kDa) subunit termed α_2/δ, which, like β subunits, enhances cell surface expression and modulates the biophysical properties of channel heteromers [1], [6], [7]. Since multiple genes encode each type of Ca_v subunit and their transcripts undergo RNA splicing, Ca_vs manifest a considerable potential for diversity not only in terms of biophysical function, but also in their modulation and cellular expression patterns [1], [7].

Irrespective of their location, emerging data has shown that Ca_vs are organised into large heterogeneous macromolecular assemblies containing a plethora of signal transduction proteins with which they interact and co-operate to meet local and global functional demands [4], [8], [9], [10]. Defining the mechanisms by which such assemblies are constructed and distributed is therefore crucial to understanding and manipulating Ca_v function [10], [11], [12]. In this regard, an important step forward has been the observation that Ca_v proteins co-localise with components of specialised cholesterol-rich membrane signalling domains termed lipid rafts [13], [14], in both heterologous expression systems and native tissues [15–21]. While alterations in Ca_v currents seen with cholesterol-depleting agents argue that raft-association is physiologically significant, the precise effects appear to be subtype and/or tissue specific [16], [18–21]. Although different Ca_vs may associate with rafts using alternate modalities [18], [22], there is now compelling evidence for a major involvement of the α_2/δ subunit [18], [20], [21]. Thus, α_2/δ subunits co-localise with the lipid raft marker proteins caveolin and flotillin when expressed alone [18], [20], [21] and are also

necessary and sufficient for the targeting of $Ca_v2.2$ complexes to rafts [21].

Until recently, how the α_2/δ subunit might mediate Ca_v raft targeting was unclear. Structurally, the α_2/δ subunit has been viewed as a type I transmembrane (TM) spanning protein (Fig. 1A) composed of a large exofacial α_2 head region linked via disulfide bonds to a smaller membrane associated δ subunit [1], [7], [23], [24], [25]. Owing to the presence of features such as Von Willebrand factor A (VWA) and Cache domains, commonly found in integrins and other cell surface proteins, the α_2 region is thought to have a modular structure [6], [7], [26] affording interactions with extracellular matrix proteins such as thrombospondin [27]. Structure-function analysis has also shown that the α_2 region mediates those interactions with Ca_vs that support current enhancement and the biophysical effects seen upon co-expression of α_2/δ subunits with α_1/β complexes [28], [29]. In contrast, the δ polypeptide, while affecting the voltage-dependence of Ca_vs [28], has been viewed as primarily providing a means for attaching the α_2 polypeptide to the cell surface via its hydrophobic putative TM-spanning domain located proximal to the short, intracellular, carboxy terminus [1], [7], [20][23–25]. However, a recent study has challenged this structural model and offered a new mechanism for Ca_v raft localisation by suggesting the α_2/δ subunit associates with the plasma membrane via a glycosylphosphatidylinositol (GPI) anchor attached to the δ polypeptide [20]. In common with other GPI anchored proteins, GPI attachment is envisaged to occur through the action of an ER-resident GPI-transamidase which recognises, cleaves and modifies a motif located at the distal carboxy terminus [28], [30–32]. While such anchoring motifs do not have a strict consensus sequence, they contain common elements including a) an amino acid with a small side chain (notably G, C, D, A, N or S) known as the ω site/residue, to which the GPI moiety is amide-linked, b) two adjacent residues (ω+1..2) with small side chains (typically G, A and S), c) a spacer sequence of >6 hydrophilic residues, commencing at the ω+3 position and d) a stretch of hydrophobic residues (particularly L) capable of spanning the membrane [30], [31].

Since GPI-anchored proteins are highly concentrated in lipid rafts [14], [33], [34], the revised model of α_2/δ subunit structure has then been used to rationalise Ca_v raft targeting [20], [35] and the apparent weakness of the α_2/δ subunit-α_1/β complex interaction [10], [36]. However, while seeming attractive in offering GPI attachment as a further regulatory locus [35], such a model requires that lipid-lipid interactions between a single δ subunit GPI anchor and liquid-ordered (L_o) raft lipids [37] can specify the raft association of $Ca_v\alpha_1$ (+β), a large, multispanning, membrane protein complex, predicted to partition into liquid-disordered (L_D), bulk phase lipid [14], [38], [39]. Moreover, of the four mammalian α_2/δ subunits, only α_2/δ-3 shows a significant potential for GPI anchoring when analysed by predictive algorithms (Table 1). Recent evidence also indicates that the co-localisation of raft markers and α_2/δ-1 subunits (when expressed alone or with α_1/β complexes) in cell surface aggregates demands an intact actin-based cytoskeleton [21]. However, while this is consistent with a role for actin in shaping the distribution and dynamics of GPI-anchored proteins [40], [41], [42], such observations are equally consistent with the hypothesis that α_2/δ-1 subunits reside in rafts, and/or higher order raft assemblies, via organising principles based upon protein-protein [21], [42], [43], [44] and/or specialised lipid-protein [14], [45], [46], [47] interactions.

To resolve the above hypotheses we have re-visited the raft localisation of the α_2/δ subunit using an established strategy [48], [49], [50] based on the expression of chimera, where the reported GPI-anchoring sequences in α_2/δ-1 have been swapped with those from a known Type I TM-spanning protein – PIN-G (Fig. 1B) [51]. Like its α_2/δ-2 and α_2/δ-3 counterparts, α_2/δ-1 has been described as a GPI-anchored protein [20]. However, unlike α_2/δ-2 and α_2/δ-3, the consequences of mutating the presumptive GPI-anchoring motif on α_2/δ-1 raft localisation or Ca_v currents have not been reported. Using imaging, electrophysiological and biochemical assays that we recently employed to analyse α_2/δ-1 in rafts [21], we now show that the raft localisation of α_2/δ-1 is preserved even after replacement of the reported GPI anchoring motif with the TM domain of PIN-G. Conversely, the GPI-anchoring motif is not sufficient to target PIN-G to lipid rafts. While the localisation of a PIN construct containing α_2/δ-1, and its GPI motif, to lipid rafts shows susceptibility to GPI-cleavage using phosphoinositide-specific phospholipase C (PI-PLC), this effect is assay-dependent and seems to lack specificity as it also disrupts the raft localisation of caveolin, but, interestingly, not flotillin. Our data therefore support a model where the raft localisation of α_2/δ-1 depends upon exofacial sequences upstream and independent of the putative GPI-anchoring motif.

Results

Construction and GPI-anchoring potential of α_2/δ-1/PIN-G chimera

To dissect the role of GPI anchoring in localising α_2/δ subunits to lipid rafts, a series of chimera were prepared between rat α_2/δ-1 and PIN-G, a functionally inert Type I TM protein reporter that lacks trafficking or post-translational modification motifs [51] (Fig. 1). Initially, we made a PIN chimera −PIN-α_2/δ - encoding the PIN 'head' region (i.e. signal peptide, Haemagglutin (HA) and Green fluorescent protein (GFP) tags, lacking TM and intracellular domains) fused to full length α_2/δ-1. Next, a chimera −PIN-δ_c - was generated by fusing the PIN head to the distal carboxy terminal region of the δ-1 polypeptide to yield a construct containing the entire purported GPI-anchoring motif of α_2/δ-1, plus 33 residues upstream, and all residues downstream of the ω site (Wild type (WT) α_2/δ-1:Gly1060, [20]. Two additional constructs −PIN-δ_c-PIN_{TMI} and PIN-α_2/δ-PIN_{TMI} – were then designed where the putative GPI anchoring motifs within PIN-δ_c and PIN-α_2/δ were disrupted by replacement of all δ residues after the ω residue, with those encoding the transmembrane and intracellular region ('TMI' residues 327–370) of PIN-G. Based upon the work of Davies et al., 2010 [20] both the PIN-α_2/δ and PIN-δ_c constructs are predicted to be GPI anchored by virtue of the presence of the purported α_2/δ-1 GPI-anchoring motif. However, this prediction is supported by only one (Pred-GPI) of the three independent algorithms [30], [52], [53] we employed, and even then with GPI-attachment at a different ω residue to that predicted by Davies et al., [20] (Table 1). In contrast, all three algorithms predict that PIN-G, PIN-δ_c-PIN_{TMI} and PIN- α_2/δ-PIN_{TMI} are not GPI-anchored (Table 1), whereas GFP-GPI, which contains the GPI-anchoring motif of the folate receptor [54] is GPI-anchored.

The biophysical properties of PIN-α_2/δ are retained following substitution of the GPI-anchoring motif with the transmembrane and intracellular sequence of PIN-G

In order to confirm that PIN-$\alpha_2\delta$ was fully functional we compared its effects on the electrophysiological properties of $Ca_v2.2/\beta_{1b}$ channels, with those of WT $\alpha_2\delta$-1. Preliminary experiments indicated that the presence of the GFP-tag on PIN-$\alpha_2\delta$ caused a marked hyperpolarisation of the V_{50} for activation and a slowing of both current activation and inactivation (Fig. S1).

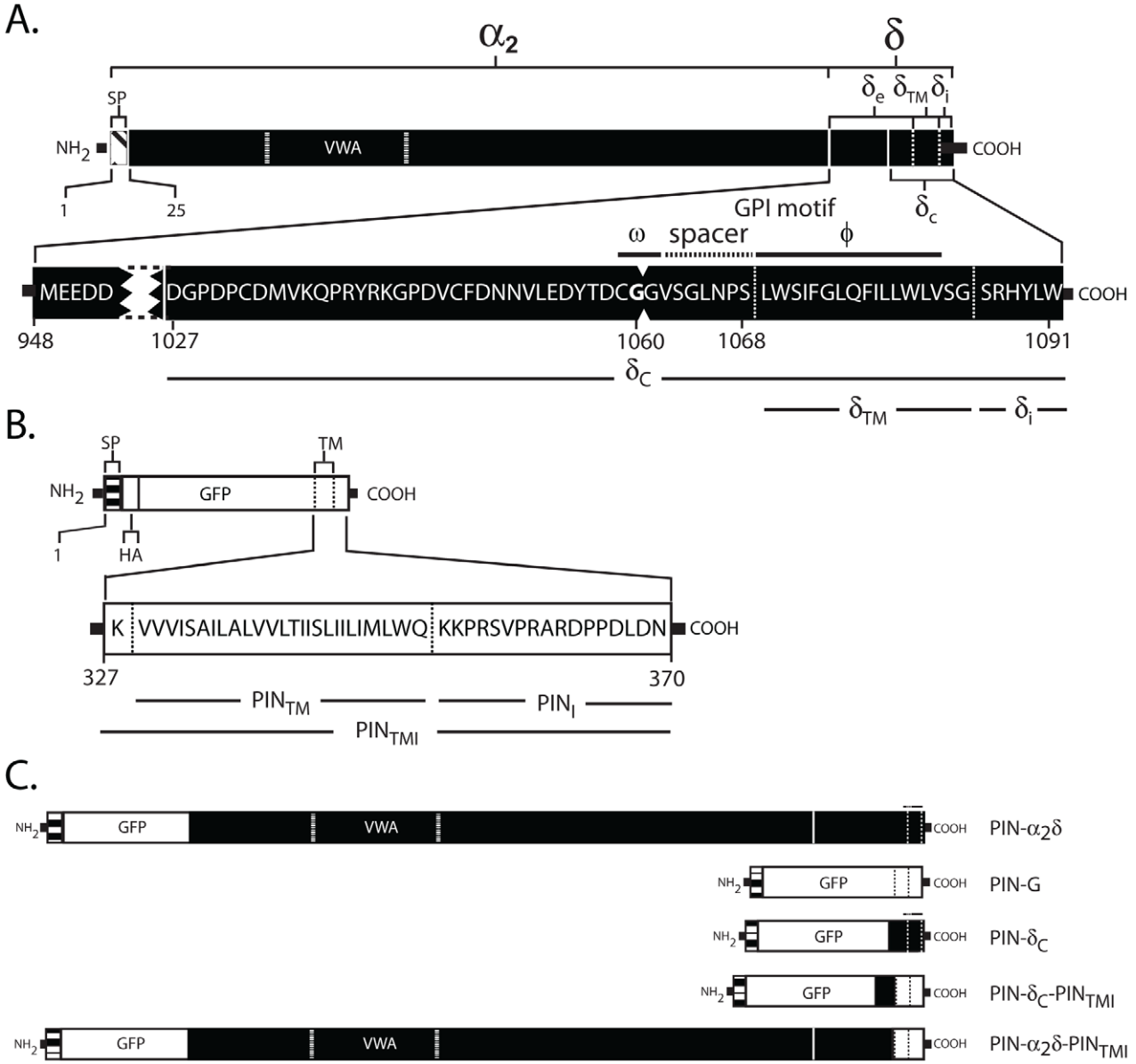

Figure 1. Depiction of WT α_2/δ-1 (A), the PIN-G reporter (Genbank AY841887.1) [51] (B) and chimeric (C) constructs. Throughout, numbering is based on the full-length polypeptide prior to signal peptide cleavage and cartoons for all constructs are approximately to scale. A. Wild type α_2/δ showing positions of the α_2 and δ polypeptides and Von Willebrand factor A (VWA) domain. In α_2/δ-1, residues 1–25 encode the signal peptide (SP). The δ subunit is further subdivided into exofacial (δ_e), putative transmembrane (δ_{TM}) and intracellular (δ_i) regions. The putative minimal GPI anchoring motif, located within a cysteine-rich region (δ_c) proximal to the external face of the lipid bilayer, contains, in turn, the ω residue (Gly1060) to which GPI is attached, a short spacer (dashed line) and a largely hydrophobic region. Indents between residues 1060 and 1061 indicate chimera fusion site where all downstream δ sequences in constructs PIN-δ_c or PIN-α_2/δ were replaced by the transmembrane and intracellular carboxy terminal residues of PIN-G (constructs PIN-δ_c-PIN_{TMI} and PIN-α_2/δ-PIN_{TMI}). The parent construct PIN-G (B) contains a signal peptide derived from the Igκ chain, an exofacial haemagglutin (HA) epitope tag, green fluorescent protein (GFP) a carboxy terminal sequence (PIN_{TMI}) containing the transmembrane spanning domain from the platelet-derived growth factor receptor and a 17 residue intracellular inert region, whose modification with endocytic or other cytoplasmically exposed targeting motifs can be used to re-direct the reporter to specific intracellular organelles [51]. Chimera (C) include PIN-δ_c, where the entire transmembrane and intracellular region (Residues 327–370) of PIN-G was replaced by WT α_2/δ residues 1027–1091 (i.e. δ_c, δ_{TM}, δ_i); PIN-δ_c-PIN_{TMI} corresponding to a PIN-G construct containing δ_c residues (1027–1060) inserted prior to the PIN_{TMI} region. Additional chimera include PIN-α_2/δ, corresponding to exofacial PIN-G residues 1–326 fused to the amino terminus of WT α_2/δ-1, and PIN-α_2/δ-PIN_{TMI}, where the C-terminal residues (WT α_2/δ-1: 1061–1091 (see A)) were replaced by the entire transmembrane and intracellular region (Residues 327–370) of PIN-G. While the putative GPI anchoring motif (lines in C) is present in PIN-δ_c and PIN-α_2/δ, it is absent in PIN-G and disrupted in PIN-δ_c-PIN_{TMI} and PIN-α_2/δ-PIN_{TMI} chimera. Vertical solid and dashed lines denote α_2/δ and transmembrane domain boundaries, respectively.
doi:10.1371/journal.pone.0019802.g001

These effects are consistent with previous reports on the biophysical effects of amino-terminal modifications of the α_2/δ subunit [55]. As a result, all subsequent electrophysiological experiments were conducted using constructs that lacked the GFP tag (deGFP; Fig. S1). As shown in Fig. 2, co-expression of PIN-$\alpha_2\delta$ conferred on $Ca_v2.2/\beta_{1b}$ currents the typical hallmarks associated with the presence of WT $\alpha_2\delta$-1. Thus, compared with $Ca_v2.2/\beta_{1b}$ in the absence of $\alpha_2\delta$-1, the peak current density, I_{max}, was

Table 1. Comparison of predicted GPI-anchoring potential for WT $\alpha_2\delta$-1, PIN-$\alpha_2\delta$ chimera, mutant $\alpha_2\delta$-2 GAS:WKW and Thy-1.

Protein	BIG-PI	FragAnchor	PredGPI
WT $\alpha_2\delta$-1	No (−26.06; P = 0.039; CG**G**V)	Rejected (NN 0.491)	Probable (CGG**V**)
WT $\alpha_2\delta$-2	No (−46.37; P = 0.2; G**A**SF)	Rejected (NN 2.8×10^{-5})	Not GPI-anchored
WT $\alpha_2\delta$-3	Yes (+8.86; P = 3.1×10^{-4}; E**C**GG)	Accepted (NN 0.999)	Highly probable (**E**CGG)
WT $\alpha_2\delta$-4	No (−7.03; P = 4.8×10^{-3}; **N**AQD)	Probable (NN 0.989)	Probable (D**C**GG)
PIN-G	No (−85.82; P = 0.87; R**S**VP)	Rejected (NN 3×10^{-6})	Not GPI-anchored
PIN-$\alpha_2\delta$	No (−26.06; P = 0.039; CG**G**V)	Rejected (NN 0.491)	Probable (CGG**V**)
PIN-$\alpha_2\delta$ -PIN_{TMI}	No(−85.82; P = 0.87; R**S**VP)	Rejected (NN 3×10^{-6})	Not GPI-anchored
PIN-δ_C	No (−26.06; P = 0.04; CG**G**V	Rejected (NN 0.491)	Probable (CGG**V**)
PIN-δ_C-PIN_{TMI}	No (−85.82; P = 0.87;R**S**VP)	Rejected (NN 3×10^{-6})	Not GPI-anchored
$\alpha_2\delta$-2 GAS:WKW	No (−51.73; P = 0.28; P**S**LG)	Rejected (NN 1.1×10^{-5})	Not GPI-anchored
Thy-1	Yes (+11.44; P = 1.7×10^{-4}; **C**GGI)	Accepted (NN 0.999)	Highly probable (**C**GGI)
GFP-GPI	Yes (+11.75; P = 1.57×10^{-4}; AM**S**G)	Accepted (NN 0.999)	Highly probable (AM**S**G)

Proteins were analysed using three independent algorithms Big-PI [30] (http://mendel.imp.ac.at/gpi/gpi_server.html), FragAnchor [55] (http://navet.ics.hawaii.edu/~fraganchor/NNHMM/NNHMM.html) and PredGPI [56] http://gpcr.biocomp.unibo.it/predgpi/). Big-PI is a predictor based on scoring the presence of an amino terminal signal peptide and features of canonical carboxy-terminal GPI-anchoring motifs. FragAnchor identifies GPI motifs using a Neural Network (NN) and Hidden Markov Model (HMM). PredGPI integrates a Support Vector Machine and HMM and employs accurately trained datasets. Likelihood of GPI anchoring is indicated by positive scores in Big-PI, NN values ≈1 in Frag Anchor and a ranking (Highly probable, probable, lowly probable and not GPI-anchored) in PredGPI. Of the three algorithms only Big-PI and PredGPI predict ω-site residues (bold and underlined in tetrapeptide sequences indicated), with the latter reported to afford the lowest rate of false positive predictions. Note that the ω-site residues giving the highest potential for GPI-modification are indicated, irrespective of the protein's potential for GPI modification. While differences exist in the predicted ω-site residues obtained between algorithms, these are generally in very close physical proximity. Of the four WT Ca_v-$\alpha_2\delta$ subunits only $\alpha_2\delta$-3 is predicted to be GPI-anchored by all three algorithms while WT $\alpha_2\delta$-1 is only predicted to be, using PredGPI. In addition, the predicted ω-site for WT $\alpha_2\delta$-1 differs between algorithms (Big-Pi: CG**G**V; PredGPI: CGG**V**) and also to that reported [20](C**G**GV).
doi:10.1371/journal.pone.0019802.t001

enhanced approximately 4-fold, the V_{50} for activation was hyperpolarised by some 13 mV on average and the rate of current inactivation was enhanced (decreased τ_{inact}) upon co-expression of PIN-$\alpha_2\delta$ (see also Table S1). We next examined the functional effects of disrupting the GPI anchoring motif within $\alpha_2\delta$. Somewhat surprisingly, and in contrast to data for the $\alpha_2\delta$-2 and $\alpha_2\delta$-3 GPI-anchoring-deficient mutants [20], co-expression of PIN-α_2/δ-PIN_{TMI} with $Ca_v2.2/\beta_{1b}$ produced identical currents to those of channels containing either PIN-$\alpha_2\delta$ or WT $\alpha_2\delta$-1. In the absence of any α_2 sequences there was no functional effect on $Ca_v2.2/\beta_{1b}$ channels (Table S1; PIN-δ).

Formation of α_2/δ puncta is independent of the GPI-anchoring motif

Upon expression in COS-7 cells and surface anti-HA immunostaining, PIN-α_2/δ exhibited a labelling pattern (Fig. 3A) characterised by the appearance of numerous small puncta, spread randomly over the cell surface, and matching that of WT α_2/δ-1

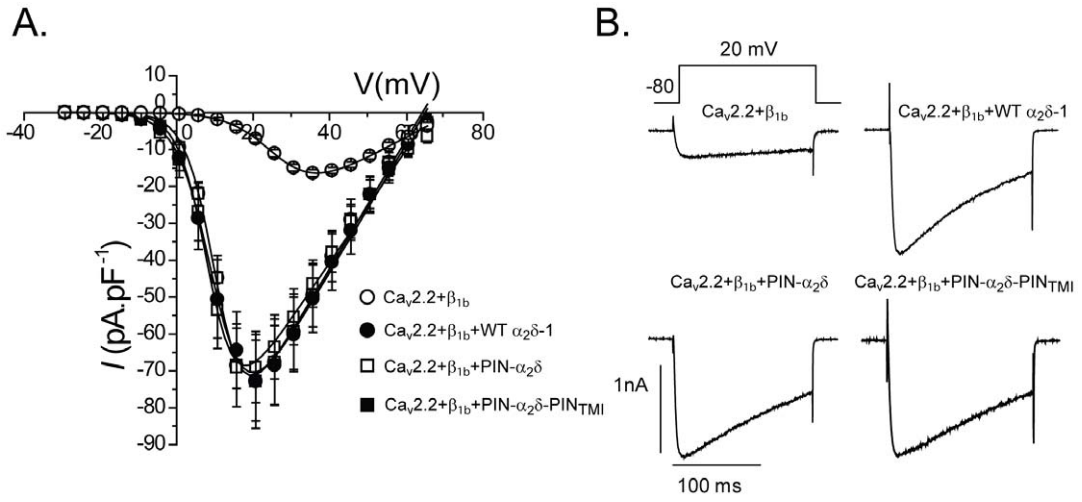

Figure 2. Effect of WT $\alpha_2\delta$-1, PIN-$\alpha_2\delta$ and PIN-$\alpha_2\delta$-PIN_{TMI} on $Ca_v2.2/\beta_{1b}$ currents. *(A)*Average current density-voltage (*I-V)* plots for $Ca_v2.2/\beta_{1b}$ currents in the absence of α_2/δ-1 (open circle) and in the presence of WT α_2/δ-1 (closed circle), PIN-$\alpha_2\delta$ (open square) and PIN-$\alpha_2\delta$-PIN_{TMI} (closed square). Continuous lines indicate the Boltzmann fits to *I-V* plots using the function described in the Methods. *(B)* Representative peak current traces from cells expressing $Ca_v2.2/\beta_{1b}$ in the absence of $\alpha_2\delta$-1 and $Ca_v2.2/\beta_{1b}$ co-expressed with WT $\alpha_2\delta$-1, PIN-$\alpha_2\delta$ and PIN-$\alpha_2\delta$-PIN_{TMI}. Currents were evoked using 150 ms depolarising steps in 5 mV intervals (−30 to +65 mV), from a holding potential, V_h, −80 mV. Data are shown as the mean ± S.E.M.
doi:10.1371/journal.pone.0019802.g002

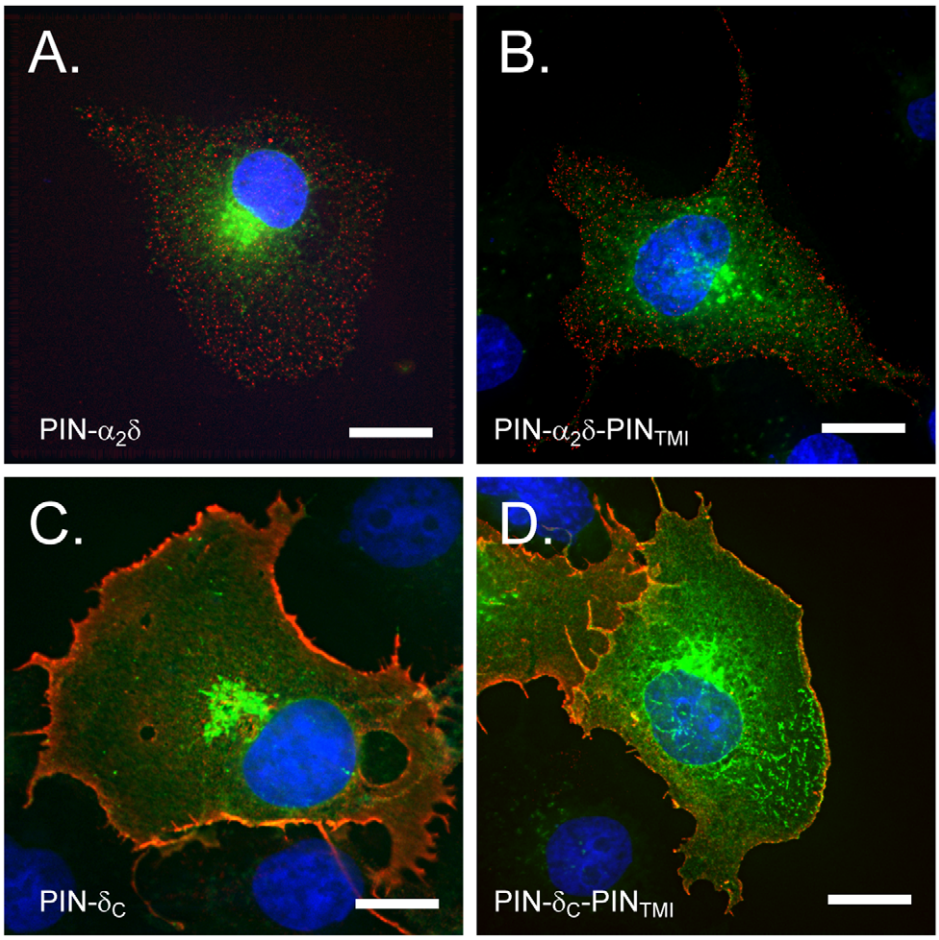

Figure 3. Surface and total cellular distribution of PIN-α_2/δ chimera expressed in COS-7 cells. A. PIN-α_2/δ. B. PIN-α_2/δ-PIN_{TMI}. C. PIN-δ_c. D. PIN-δ_c-PIN_{TMI}. Cells were labelled with anti-HA and Cy5 secondary antibodies using a surface-labelling specific protocol (Methods) and the distribution of surface (red) and total (green, GFP) PIN construct expression determined by fluorescence imaging. Note strong labelling at cell margins for PIN-δ_c and PIN-δ_c-PIN_{TMI} and highly punctate labelling for PIN-α_2/δ and PIN-α_2/δ-PIN_{TMI}. Scale bar 15 μm.
doi:10.1371/journal.pone.0019802.g003

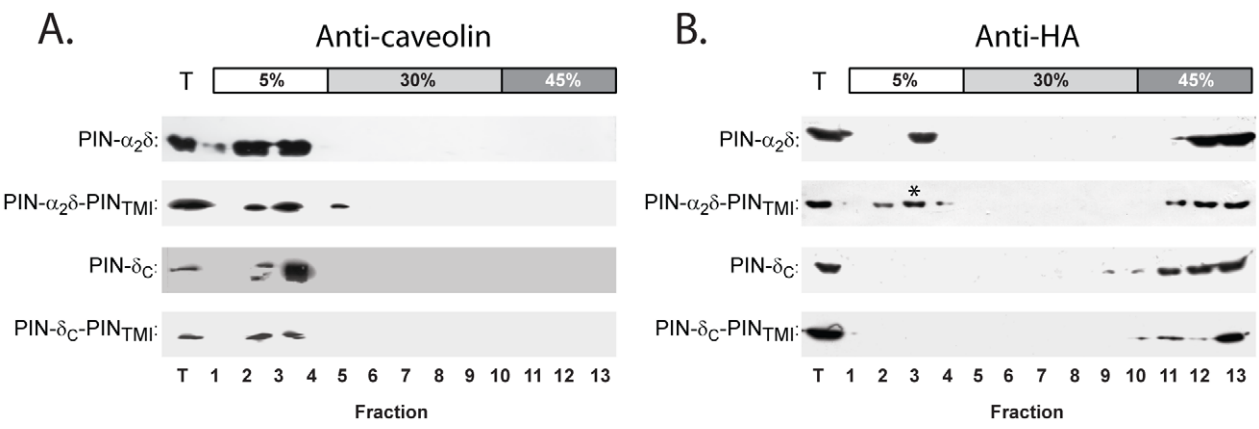

Figure 4. Distribution profile of PIN-α_2/δ chimera in detergent-resistant membranes is not affected by disruption of the putative GPI anchoring motif. COS-7 cells were transfected with the corresponding PIN chimera and the membranes analysed via immunoblotting of fractions from sucrose density gradients containing 1% Triton-X-100, using antibodies to caveolin (endogenous) (Panel A) or anti-HA (Panel B)(for PIN chimera). Representative blots in panels A and B, correspond to cells transfected with PIN-α_2/δ, PIN-α_2/δ-PIN_{TMI}, PIN-δ_c and PIN-δ_c-PIN_{TMI}. Note the absence of PIN-δ_c or PIN-δ_c-PIN_{TMI} in raft fractions (3–6) and the presence in raft fractions of both PIN-α_2/δ and PIN-α_2/δ-PIN_{TMI} (asterisk in B). Immunodetection loading controls are denoted by 'T'.
doi:10.1371/journal.pone.0019802.g004

[21]. In contrast, such puncta were absent in cells expressing PIN-δ_c (Fig. 3C) Rather, PIN-δ_c labelling was distributed evenly over the cell surface and at the cell margins. Significantly, the two different patterns of labelling seen between PIN-α_2/δ and PIN-δ_c were retained in the derivative PIN-α_2/δ-PIN$_{TMI}$ (Fig. 3B) and PIN-δ_c-PIN$_{TMI}$ (Fig. 3D) constructs, where the GPI anchoring motifs had been disrupted.

Raft localisation requires α_2/δ sequences upstream of the GPI-anchoring motif

Elsewhere, we have shown an intimate link between the formation of puncta and the co-localisation of α_2/δ with lipid raft proteins [21]. Consequently, the presence of puncta in constructs lacking the putative GPI anchoring motif (PIN-δ_c-PIN$_{TMI}$ and PIN-α_2/δ-PIN$_{TMI}$) and *vice versa* (PIN-α_2/δ and PIN-δ_c), prompted us to examine and compare their raft localisation more directly. To this end, we exploited the ability of lipid raft components, including α_2/δ subunits [18], [20], [21], to migrate into low density fractions upon equilibrium centrifugation of cell lysates in sucrose density gradients containing ice-cold non-ionic detergents [14], notably Triton-X-100 [15], [56], [57]. Following centrifugation of lysates prepared at 48 h post-transfection, gradients were fractionated and fractions immunoblotted using anti-HA antibodies (Fig. 4). To control for gradient fidelity, each fraction was also analysed for the presence of the raft marker caveolin. Irrespective of the transfection condition, endogenous caveolin (22 kDa isoform) was detected as a single peak in fractions corresponding to the 5%–30% sucrose interface (Fig. 4A). In cells transfected with PIN-α_2/δ (Fig. 4B blot i) approximately 20% of the anti-HA immunoreactivity was distributed at the 5–30% interface in caveolin-positive fractions, with the remainder locating to fractions of higher density centred on the 30–45% sucrose interface. In contrast, PIN-δ_c – which contains the putative GPI motif – was localised exclusively in the higher density non-raft fractions (Fig. 4B blot iii). Next we examined the distributions of constructs PIN-α_2/δ-PIN$_{TMI}$ (Fig. 4B blot ii) and PIN-δ_c-PIN$_{TMI}$ (Fig. 4B blot iv) - which lack the putative GPI-motif. In both cases raft/non-raft distributions of HA-immunoreactivity were the same as their parent constructs (PIN-α_2/δ: raft + non-raft and PIN-δ_c: non-raft, respectively). Thus, the raft localisation of PIN-α_2/δ appears independent of the GPI motif. Conversely, the presence of the GPI motif in PIN-δ_c is insufficient to support raft localisation, implying that upstream sequences are required.

The expression of PIN-α_2/δ cell surface puncta is resistant to PI-PLC treatment

Taken together, these data contradict the notion that the association of α_2/δ-1 with lipid rafts is specified by the proposed GPI-anchoring motif [20]. To examine this issue further we tested for the existence of a GPI anchor through its susceptibility to PI-PLC cleavage [20], [58], [59]. First, we followed the approach of Davies et al., (2010) [20] who used imaging to assay the effect of PI-PLC on the surface expression of α_2/δ constructs. For comparison we also examined the surface and total (surface + intracellular) distribution of GFP-GPI, a well-defined GPI-anchored green fluorescent protein [54]. As shown in Fig. 5A–D, GFP-GPI was found throughout the cell where it was localised in both tubulovesicular structures and at the cell surface. Although known to reside in lipid rafts like other GPI-anchored proteins [54], [59], [60], GFP-GPI surface labelling was not present in the well-defined puncta seen with PIN-α_2/δ (e.g. Fig. 3), but rather it was distributed over the cell surface in a pattern reminiscent of a very fine, granular, meshwork (Fig. 5C,D). Following treatment with PI-PLC, all GFP-GPI-transfected cells showed a qualitative decrease in surface (Cy5/anti-GFP) labelling intensity and distribution compared with non-PI-PLC-treated cells (Fig. 5G–J). More quantitative comparisons based on determining the 'on cell' signal to noise ('off cell' background) ratio (S/B) of raw (i.e. non-background subtracted) images, showed that PI-PLC caused a reduction in GFP-GPI surface labelling intensity to 23% of control (i.e. −PI-PLC) levels ($(S/B)-1 = 0.44\pm0.066$ $n=8$ (−PI-PLC) vs $(S/B)-1 = 0.10\pm0.0217$ $n=8$ (+PI-PLC); $p=0.0002$) (Fig. 5K). In parallel, we examined the action of PI-PLC on the surface expression of PIN-α_2/δ. In contrast to GFP-GPI, and as noted above, PIN-α_2/δ showed a pattern of surface labelling comprised of numerous high intensity puncta, with little interstitial (inter-punctal) labelling (Fig. 5L–O). Significantly, however, pre-treatment of cells with PI-PLC had no apparent effect on the labelling intensity ($(S/B)-1 = 0.75\pm0.18$ $n=6$ (−PI-PLC) vs 0.95 ± 0.27 $n=8$ (+PI-PLC), $p=0.56$) (Fig. 5 R–V and Fig. S2). Equally important, using detailed particle analysis we found no effect on the dimensions or density of the PIN-α_2/δ puncta (Fig. S2). Neither the number of particles of given area (size distribution)(Fig. S2A), nor the particulate area fraction (a measure of changes in particle dimension) (Fig. S2B) were affected by PI-PLC treatment. Thus, we found no evidence for the effects predicted were PI-PLC treatment able to induce either 'stripping' (i.e. decreased particle size), disassembly (formation of smaller puncta) or both (Fig. S2C–F).

The raft distribution of both PIN-α_2/δ and caveolin in sucrose gradients is altered by PI-PLC treatment

As a further test for the presence of a GPI anchor in PIN-α_2/δ, we examined the effect of PI-PLC on the partitioning of PIN-α_2/δ in lipid raft fractions obtained using equilibrium centrifugation in sucrose gradients containing ice-cold Triton-X-100. As shown in Fig. 6, gradient analysis of lysates from cells expressing GFP-GPI (Fig. 6A, blot i) showed anti-GFP immunoreactivity exclusively in lipid raft fractions at the 5–30% sucrose interface. In contrast, lysates from cells pre-treated with PI-PLC (Fig. 6B, blot i) showed a marked shift in immunoreactivity which was now present in higher density non-raft fractions. Next, we examined lysates from cells transfected with PIN-α_2/δ. As before (Fig. 4), anti-HA immunoreactivity was detected in both the raft and non-raft fractions ((Fig. 6A, blot ii). However, following pre-treatment of cells with PI-PLC all the anti-HA immunoreactivity appeared in the higher density, non-raft fractions (Fig. 6B, blot ii). While these data supported the contention that PIN-α_2/δ is GPI-anchored [20], it was also possible that PI-PLC might have a more globally disruptive effect on lipid raft integrity, particularly given the lack of effect of molecular disruption of the GPI anchoring motif. To examine such a possibility we, therefore, examined the effect of PI-PLC on the gradient distribution of both caveolin (Fig. 6A,B, blot iii) and flotillin (Fig. 6A,B, blot iv) - two endogenous raft markers with separate and independent modes of raft association [61], [62], which both co-localise in puncta containing α_2/δ [21]. As anticipated, both caveolin (Fig. 6A, blot iii) and flotillin (Fig. 6A, blot iv) were concentrated in raft fractions in the absence of PI-PLC pre-treatment. However, following PI-PLC pre-treatment, the distribution of caveolin (Fig. 6B, blot iii), but not flotillin (Fig. 6B, blot iv), shifted such that it was found primarily in the higher density non-raft fractions. Thus, PI-PLC appears to have a generally disruptive effect on the integrity of lipid rafts, whose detection depends upon whether caveolin or flotillin is used as a marker.

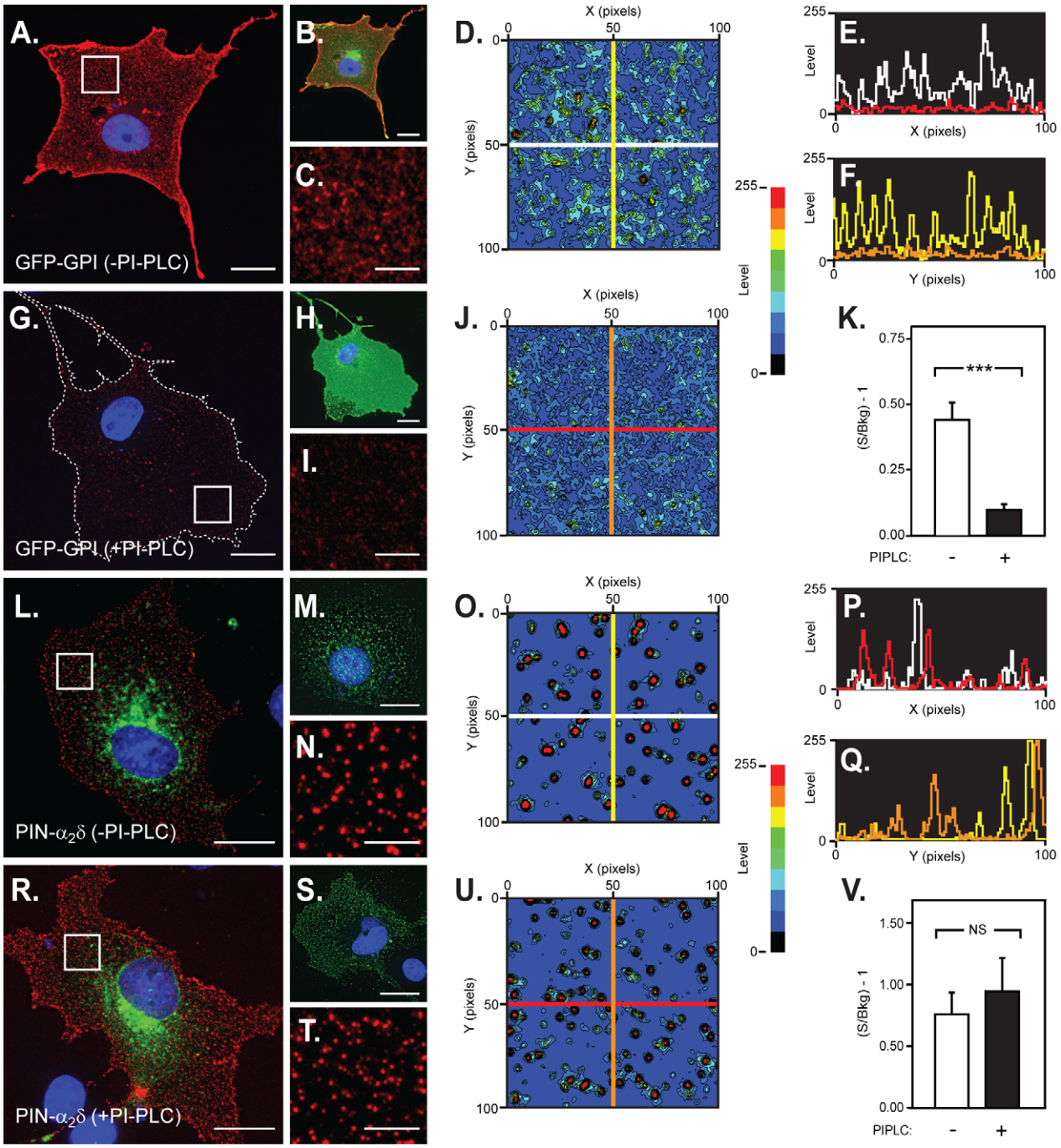

Figure 5. Effect of PI-PLC cell pre-treatment on the cell surface distribution of GFP-GPI (control) and PIN-α_2/δ expressed in COS-7 cells. Panels A–I correspond to GFP-GPI fluorescence in the absence (A–C) and presence (G–I) of PI-PLC cell treatment. For clarity, panels A and G depict just the surface (red channel, anti-GFP) labelling corresponding to the merged (red (surface) and green (GFP, surface + intracellular) images shown in B and H. Panels C and I correspond to high magnification views of the boxed areas shown in A and G, respectively. Note strong surface labelling and evidence of clustering of GFP-GPI, in the absence of PI-PLC and diminution of surface cluster and interstitial fluorescence after PI-PLC treatment. Since contiguity between GFP-GPI clusters precluded standard particle analysis, the effect of PI-PLC on GFP-GPI clustering was analysed further by generating contour maps (panels D and J) (level scale (0–255) shown to right) of the labelling seen in panels C and I, respectively. Line scans based on the contour maps were then constructed to show differences in fluorescence intensity in the absence (white and yellow in D and F) or presence (red and orange in D and F) of PI-PLC cell treatment. Panel K shows the effect of PI-PLC cell pre-treatment on the signal to background fluorescence for raw images ($n>8$) collected using identical imaging conditions. *** denotes statistically significant difference ($P<0.001$); Student's t-test. Panels L–T correspond to images from cells transfected with PIN-α_2/δ in the absence (L–N) and presence (R–T) of PI-PLC. Panels L and M (−PI-PLC) and R and S (+PI-PLC) show merged images for total (surface + intracellular)(green, GFP) and surface (red, anti-GFP)) for separate cells. Panels N and T correspond to high magnification views of the boxed areas shown in L and R (red, (surface) channel only). Note the presence of extensive PIN-α_2/δ clustering irrespective of whether or not the cells had been treated with PI-PLC. Panels O and U correspond to contour maps (above) of the labelling seen in panels N and T, respectively (level scale (0–255) shown to right). Line scans corresponding to the contour maps were then constructed to show differences in fluorescence intensity in the absence (white and yellow in P and Q) or presence (red and orange in P and Q) of PI-

PLC cell treatment. Panel V shows the effect of PI-PLC cell pre-treatment on the signal to background fluorescence for raw images (n>8) collected using identical imaging conditions. Note lack of effect of PI-PLC on PIN-α_2/δ distribution (O and U) or intensity (V). All images are representative examples from data sets comprised of >8 images (>2 experiments). Scale bars are as follows: panels A, B, G, H, L, M, R and S, 20 μm; panels C, I, N and T, 4 μm.
doi:10.1371/journal.pone.0019802.g005

Treatment with PI-PLC alters the cellular distribution of caveolin but not flotillin

To obtain further evidence for a generalised effect of PI-PLC on raft integrity, we examined the cellular distribution of caveolin and flotillin before and after PI-PLC treatment, using imaging assays (Fig. 7). As documented elsewhere [21], both of these raft marker proteins localise to puncta and large aggregates throughout permeabilised, non-PI-PLC-treated, COS-7 cells (Fig. 7A (caveolin), 7D (flotillin)). However, following pre-treatment of cells with PI-PLC there was a marked alteration in caveolin labelling to patterns consisting of patches of intense labelling proximal to the cell nucleus and the appearance of more diffuse labelling over the cell surface (Fig. 7B). In contrast, pre-treatment of cells with PI-PLC had no effect on the distribution of flotillin (Fig. 7E) which remained punctate throughout. These data are therefore consistent with those from the sucrose-density gradient experiments and support the notion that PI-PLC – a primary tool for defining α_2/δ-1, 2 and 3 as GPI-anchored proteins [20] - has indirect effects which may confound the assignment of proteins as possessing GPI anchors.

Discussion

In this study we have tested the notion that the $Ca_v\alpha_2/\delta$-1 subunit is a GPI anchored protein, by substitution of the putative GPI-anchoring motif, including the downstream sequence formerly designated as TM-spanning, with a *bona fide* [51] TM-spanning and intracellular sequence from the trafficking reporter, PIN-G. Using fundamentally different algorithms, each chimera is predicted to have little or no GPI anchoring potential, due to direct disruption of all residues adjacent and subsequent to the putative ω+1 site and the extended intracellular domain. By replacing the GPI-anchoring motif with bulky lysine and hydrophobic amino acids throughout, our chimera, therefore, represent an even more extensive alteration of both the motif structure and the overall GPI anchoring potential (Table 1) than that achieved previously in $Ca_v\alpha_2/\delta$-2 and Ca_v α_2/δ-3, where just three ω site residues were mutated [20]. Furthermore, by generating PIN chimera corresponding to a full length or truncated α_2/δ subunit, both containing the putative GPI-motif, it was possible to examine the independence of this motif from upstream residues.

Significantly, PIN-α_2/δ supports the key hallmarks of WT α_2/δ-1 functionality, notably a 4-fold enhancement of peak current density, a hyperpolarising shift in V_{50} for activation and an enhanced rate of inactivation, when co-expressed with $Ca_v2.2/\beta_{1b}$ subunits. Such current enhancement arises through direct actions on anterograde and retrograde trafficking of Ca_v complexes [6], [63] and is highly susceptible to post-translational modification events [55]. Thus, PIN-α_2/δ is evidently able to undergo processing and trafficking events similar to WT α_2/δ-1 and like WT α_2/δ-1, can co-assemble with $Ca_v2.2$ α_1 subunits. Equally significant, the $Ca_v2.2/\beta_{1b}$ current enhancement and kinetic features imparted by the GPI-anchor-deficient PIN-α_2/δ-PIN_{TMI} construct are identical to those of PIN-α_2/δ. This is especially remarkable given that the association of α_2/δ-1 with lipid rafts has been directly attributed to GPI-anchoring [20] and that disruption of either rafts [16], [18–21], or GPI-anchoring [20], has been reported to affect Ca_v current density. Our observation that PIN-δ does not support enhancement of $Ca_v2.2/\beta_{1b}$ currents is entirely consistent with the known requirement for sequences in the α_2 subunit [7], [28], [29].

In both our biochemical and imaging assays PIN-α_2/δ exhibits the raft-association characteristics of WT α_2/δ-1 [21]. However, in these assays PIN-δ_c - which contains the putative GPI-anchoring motif and 46 (33 δ_c and 13 GFP-linker) upstream residues between GFP and the predicted ω site (CGG) showed no raft localisation. In contrast, GFP-GPI, which contains just 22 residues between GFP and the ω site, is raft localised. Thus, raft

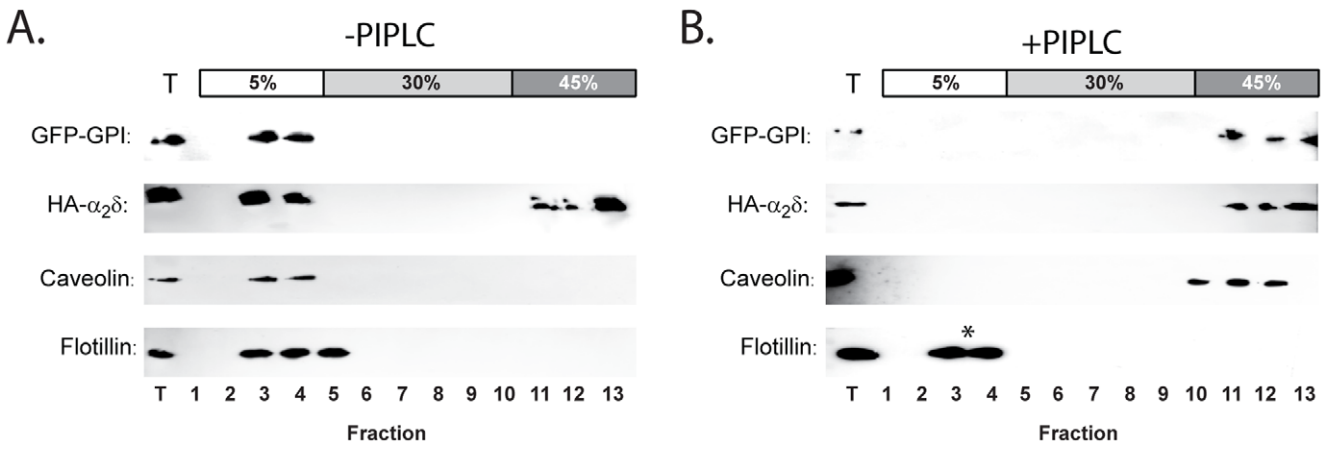

Figure 6. Effect of GPI-anchor removal through cell pre-treatment with PI-PLC. COS-7 cells were transfected with either GFP-GPI or HA-α_2/δ and the membranes analysed via immunoblotting of fractions from sucrose density gradients containing 1% Triton-X-100, using antibodies to GFP (GFP-GPI), the HA-epitope tag (HA-α_2/δ), caveolin (endogenous) or flotillin (endogenous). Representative blots at left and right correspond to cells before and after pre-treatment with PI-PLC, respectively. Note the presence of all proteins in the buoyant (raft) fraction prior to PI-PLC exposure and restriction of GFP-GPI, HA-α_2/δ and caveolin, but not flotillin (B., asterisk) in denser non-raft fractions following PI-PLC exposure. Immunodetection loading controls are denoted by 'T'.
doi:10.1371/journal.pone.0019802.g006

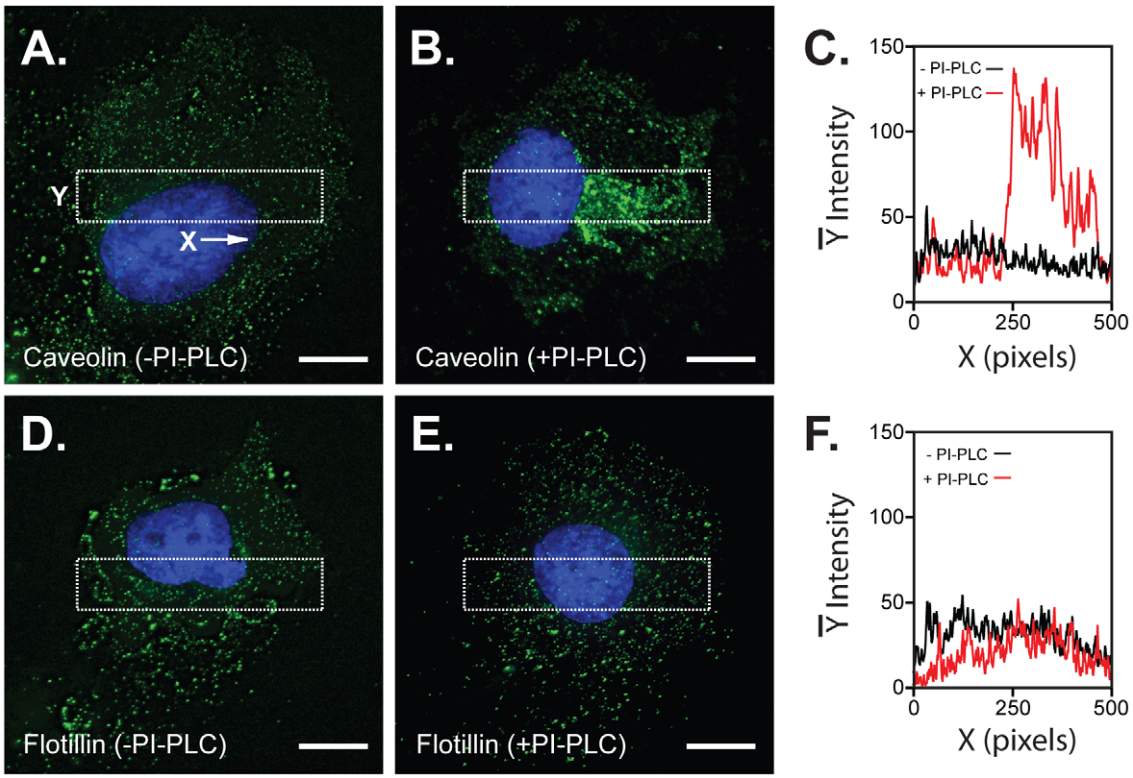

Figure 7. Effect of PI-PLC cell pre-treatment on the distribution of endogenous caveolin and flotillin in COS-7 cells. Panels A and B correspond to caveolin labelling in the absence (A) and presence (B) of PI-PLC cell pre-treatment. Panel C depicts intensity profiles (averaged in y axis) corresponding to boxes shown in A and B (red and black lines corresponding to profiles with and without PI-PLC, respectively). By averaging the fluorescence intensity, such 'box scans' reduce the noisiness seen in individual line scans. Note aggregation of caveolin fluorescence proximal to the nucleus (B) and increase in intensity (C) in images from cells pre-treated with PI-PLC. Panels D and E depict flotillin labelling in the absence (D) and presence (E) of PI-PLC cell pre-treatment. The corresponding box scans are shown in F (red line: +PI-PLC; black line: −PI-PLC). Note similarity in flotillin distribution irrespective of cell pre-treatment with PI-PLC. Scale bars: 15 μm.
doi:10.1371/journal.pone.0019802.g007

localisation must depend upon additional determinants upstream of the δ_c sequence rather than merely the number of residues upstream of the ω site. Although it is conceivable that determinants upstream of δ_c somehow promote GPI-anchor attachment, our observation that raft localisation is conserved in both PIN- α_2/δ and the anchor-deficient PIN-α_2/δ-PIN_{TMI}, argues strongly against any involvement of the putative GPI-anchor motif reported by Davies et al (2010) [20]. While we cannot rule out the possibility of cryptic (i.e. internal) GPI-anchor motifs these are very rare and are thought to resemble the classic carboxy terminal anchoring motifs in structure [64], [65]. Indeed, using predictive algorithms to assess the GPI-modification potential for sequentially truncated α_2/δ-1 constructs, we have been unable to detect any additional regions within δ-1 that could serve as obvious GPI-anchoring motifs (Fig. S3).

Notwithstanding the above, our data do not exclude the possibility that GPI-anchoring plays an indirect role in α_2/δ raft localisation. Indeed, upon treatment with PI-PLC, PIN- α_2/δ was no longer associated with lipid rafts when assessed by sucrose gradient analysis. While this effect has been interpreted as arising via the release of α_2 and regions of δ-1 up to the ω site [20] (Table 2), it appears to be non-specific since PI-PLC also prevented the raft-association of caveolin which, in contrast to GPI-anchored proteins, is localised to the inner membrane leaflet [61]. Significantly, depletion of caveolin has been reported to re-distribute Type I TM proteins from raft to non-raft fractions [66] which may explain the data reported by Davies et al., [20] where flotillin was the primary raft marker (Table 2). In support of this, our images showing that PI-PLC causes partial dispersal of caveolin, are highly reminiscent of those obtained from COS-7 cells treated with the cholesterol-depleting agent, methyl-β-cyclodextrin (M-β-CD) [21]. However, while M-β-CD also disperses flotillin and prevents its co-localisation in lipid raft fractions, PI-PLC does not. Thus, PI-PLC treatment can disrupt raft integrity, but not completely. To our knowledge, potentially disruptive effects of PI-PLC on raft structure have not been examined, although phospholipase C activity and low concentrations of its end product - diacylglycerol, are known to destabilise model membranes including those containing raft lipids [67]. Quite why caveolin and flotillin should show differential raft partitioning after PI-PLC treatment is also unclear, but likely reflects their differing modes of membrane association. While both proteins are acylated, only caveolin has a transmembrane domain [61,62,68]. Irrespective of the mechanisms, a differential effect of PI-PLC on caveolin and flotillin raft localisation, clearly, warrants caution when using these markers alone to assess raft integrity.

Taken together, our chimera studies show that Ca_v α_2/δ-1 raft localisation is independent of the putative GPI-anchoring motif and that this motif does not localise chimera to rafts. By inference, our data do not support the revised model for the topology, membrane association (i.e. GPI anchoring) or ability of α_2/δ-1 subunits to target Ca_vs to lipid rafts. Rather, raft association – at least for α_2/δ-1 - appears to require sequences upstream of the ω

Table 2. Comparison of experimental approaches and conclusions in the present study and that of Davies et al., [20].

	This study	Davies et al. [20]
A) Substrates		
Constructs	HA α_2/δ-1 (Rat), PIN α_2/δ-1 chimera	No constructs or mutants employed (point mutants in just α_2/δ-2/3)
Cell types used	COS-7	Rat DRG, Hippocampus, tsA-201 cells, cardiac muscle (data not shown)
Immunodetection	Anti-HA/Anti-GFP	Anti- α_2/δ-1
B) Evidence for GPI-Anchoring motif in α_2/δ-1		
Algorithms	Probable in only 1/3 algorithms	Not given
Other	Not inferred (see Introduction)	Inferred from α_2/δ-2, α_2/δ-3 data and partial homology.
C) Raft isolation		
Cells	COS-7 cell lysates	Hippocampal tissue lysates, tsA-201 cell lysates, cardiac muscle (data not shown)
Detergent	Triton-X-100, 4°C	Triton-X-100, 4°C
Raft markers	Endogenous Caveolin and Flotillin-1	Endogenous Flotillin-1
Conclusions	Localisation of α_2/δ-1 in rafts Raft localisation independent of GPI anchoring motif	Localisation of WT α_2/δ-1 in rafts
D) Imaging		
Cells	COS-7	Rat DRG
α_2/δ-1	Transfected constructs	Endogenous
Labelling method	Surface protocol	Non-permeabilised*
Detection	Immunofluorescence	Immunofluorescence
Quantification	Intensity and Particle analysis	Intensity
Conclusions	Formation of α_2/δ-1 puncta independent of GPI anchoring motif but requires upstream sequences	N/A
E) PI-PLC		
Concentration	4 U/ml, 1 h, 37°C	4–8 U/ml, 1 h, 37°C
Treatment - rafts	Live COS-7 cells prior to lysis	Hippocampal tissue lysates
Conclusions	Raft localisation of α_2/δ-1 reduced	Raft localisation of α_2/δ-1 reduced
Treatment - imaging	COS-7 cells, surface protocol	'non-permeabilised'* DRG cells
Conclusions	Formation of surface α_2/δ-1 puncta resistant to PI-PLC	Surface expression of α_2/δ-1 reduced by PI-PLC
F) Electrophysiology		
Constructs	$Ca_V2.2/\beta_{1b}$ +/− PIN- α_2/δ-1 chimera, or, WT-α_2/δ-1	α_2/δ-1 not tested.
Cells	COS-7	tsA-201
Conclusions	Current density unaffected by loss of GPI anchoring motif	Not tested (reduced current density in α_2/δ-2/-3 on disruption of GPI anchoring motif)

Key differences are our use of: a) both caveolin and flotillin as raft markers, b) a carefully controlled surface-labelling protocol, c) lysates from live cells treated with PI-PLC and d) the extensive use of chimera which ablate the purported GPI-anchoring motif. Asterisks denote the use of non-permeabilised cells without reference to controls. As we show elsewhere [21], fixative alone can cause significant cell permeabilisation.

doi:10.1371/journal.pone.0019802.t002

site that most likely mediate protein-protein rather than lipid-lipid interactions, a scenario more consistent with emerging views of raft biogenesis and aggregation [14], [42], [69].

Materials and Methods

Chemicals

The construct encoding wild-type rat Cav α_2/δ-1 (Neuronal splice variant; Genbank accession number: NM_012919.2) in pcDNA3.1 was supplied by T.P. Snutch (Univ. British Columbia, Canada). Rabbit $Ca_V2.2$ in pMT2 (D14157), rat $Cav\beta_{1b}$ in pMT2 (X61394) and the mut-3 variant of GFP-pMT2 (U73901) were supplied by A.C. Dolphin (University College London, UK). The pcDNA3.1 plasmid was obtained from Invitrogen, UK. Primary antibodies were obtained from the following sources: anti-α_2/δ-1 (Upstate/Millipore, UK), anti-flotillin-1, anti-clathrin, anti-GFP (Sigma-Aldrich, UK) and anti-HA (Covance, UK). Secondary antibodies were obtained as follows: FITC-conjugated anti-rabbit and anti-mouse IgGs (Jackson Immunoresearch, UK), Cy5-conjugated anti-mouse and anti-rabbit IgG (Jackson Immunoresearch, UK) and horseradish peroxidase (HRP)-conjugated anti-rabbit and anti-mouse IgGs (Dako, UK). All other reagents were obtained from Sigma-Aldrich, UK, unless stated otherwise.

Molecular biology

An α_2/δ-1 construct bearing an HA epitope tag between amino acid residues I612 and K613, was generated using a three step

strategy as described in Robinson et al. (2010) [21]. All PIN constructs were prepared through the sequential insertion, deletion or substitution [70] of specified rat α_2/δ-1 sequences into the PIN-G plasmid (Genbank: AY841887), using the QuikChange™ II kit (Agilent Technologies, UK) and mutagenic megaprimers prepared by PCR. Construct fidelity was confirmed by in-house sequencing (see Fig. 1 and Fig. S3C for chimera junctions).

Cell culture and transient transfection

Culture and transient transfection of COS-7 cells (European Cell Culture Collection, Health Protection Agency, U.K.), were carried out as described in Robinson et al. (2010) [21]. Transient transfections were performed in serum-free Dulbecco's modified Eagle's medium (DMEM) at a cell confluency of 60–70% using FuGene 6 (Roche Diagnostics, U.K.; imaging and electrophysiology) or Turbofect (Fermentas, U.K.; biochemical experiments) at a total DNA:reagent ratio of 1:3 (w/v), (total DNA: 2 μg for 6-well plates/35 mm dishes, 12 μg DNA for 10 cm plates). Transfections with $Ca_v2.2$, $Ca_v\beta_{1b}$ and $Ca_v\alpha_2/\delta$-1 used a ratio of 3:1:1 by mass of subunit cDNA. For transfections omitting α_2/δ cDNA, the α_2/δ cDNA was replaced with pcDNA3.1 to maintain the equivalent mass ratio. Cells were maintained at 37°C, 5% CO_2 in complete medium for a total of 48 hours (including any re-plating step), after which cells were: a) fixed for microscopy (below), b) re-plated onto 22 mm square coverslips for electrophysiology, or c) lysed for biochemical experiments. For re-plating post-transfection, cells were detached using a non-enzymatic cell dissociation solution (Sigma Aldrich, UK) before re-seeding in fresh complete medium.

Western immunoblotting

At 48 h post-transfection, COS-7 cells were washed in PBS and lysed at 4°C in a radio-immunoprecipitation assay (RIPA) buffer with Complete MINI EDTA-free protease inhibitor cocktail (Roche, UK). The cell lysates were then passed through a 22-gauge syringe needle 10 times to shear genomic DNA, and centrifuged at 1000 g_{av}. Supernatants were then incubated at 37°C for 15 min with Laemmli loading buffer containing 20 mM DTT and then heated to 95°C for 2 min. Sample proteins were resolved by SDS-PAGE on 10% Tris-HCl gels for 80 min at 160 V (Mini-Protean cell, BioRad, UK) and then transferred by electrophoresis (100 V for 2 h) onto nitrocellulose membranes (Whatman, UK). Air dried membranes were immersed overnight in blocking buffer (5% non-fat dry milk in Tris-buffered saline (TBS) with 0.1% Tween-20 (TTBS)), washed three times with TTBS and then incubated with the appropriate primary antibody in TTBS for 1 h at 20°C. The membranes were then re-washed with TTBS and incubated for 1 h at 20°C with the appropriate secondary HRP-conjugated antibody (1:1000) in TTBS. After further washing with TTBS, the membranes were treated with Western Lightning enhanced chemiluminescence reagent (Perkin Elmer, UK) and immunoreactive proteins detected by exposure to film (GE Life Sciences, UK).

Sucrose gradient fractionation

As we described recently [21], transiently transfected COS-7 cells were washed in PBS and lysed 48 h post-transfection with MBS (Mes-buffered saline: 25 mM Mes, pH 6.5, 150 mM NaCl) with 1% Triton-X-100 at 4°C. For a single experiment, 9×10 cm dishes were used and 150 μl of MBS/Triton-X-100 was added to lyse the cells. Cells were scraped off the dish, passed through a 22-gauge needle 10 times to shear genomic DNA and 450 μl of lysate was reserved for use as a control. The remaining 900 μl of lysate was mixed with 900 μl of 90% sucrose/MBS (w/v), placed in a 5 ml polypropylene centrifuge tube (Sorvall) and carefully overlaid with 1.5 ml of 30% sucrose/MBS, followed by 1.5 ml of 5% sucrose/MBS. Gradients were spun at 38,500 rpm (140,000 g_{av}) in a Sorvall Discovery 100SE ultracentrifuge using an AH-650 rotor for 16 h at 4°C. Post-centrifugation, 15 fractions were taken from top to bottom of the tube and analysed in subsequent Western immunoblotting. To concentrate proteins, fractions were incubated with 25% trichloroacetic acid (final), at 4°C for 30 min. Samples were centrifuged at 14,000 rpm (13,000 g_{av}) at 4°C for 20 min and the pellets washed twice with ice-cold acetone, ensuring not to disrupt the pellets. Pellets were dried at 42°C for 10 min before re-suspension in 50 μl of MBS and analysed by Western immunoblotting.

Immunocytochemistry

Cells for fluorescence microscopy were re-plated 24 hours post-transfection onto 13 mm coverslips coated with 0.01% poly-L-lysine. To preclude fixation artefacts, all imaging experiments of surface expression were performed using a two-step protocol [21]. Briefly, COS-7 cells (48 h post-transfection) were cooled on ice to 4°C and after 10 min, treated with primary antibody diluted in PBS. After 1 h at 4°C, coverslips were washed 3 times with PBS and the cells fixed with 4% (w/v) paraformaldehyde for 20 min at 20°C. Cells were then treated with the appropriate (Cy5 or FITC) fluorophore-conjugated secondary antibody for 1 h at 20°C. In order to detect intracellular epitope expression, cells were permeabilised post-fixation with 0.5% saponin for 10 min at 20°C, prior to incubation with primary antibody. Nuclear staining was performed with DAPI (4′,6-diamidino-2-phenylindole; 1 μg/ml) for 2 min at 20°C, prior to mounting with Prolong Gold Antifade reagent (Invitrogen/Molecular Probes).

PI-PLC treatment

At 48 h post-transfection, COS-7 cells were washed with serum-free DMEM and incubated with PI-PLC (Invitrogen, U.K.; 4 Units/mL) for 1 h at 37°C. The cells were then washed in DMEM to remove PI-PLC, placed on ice and processed for imaging (above) or immunoblotting.

Fluorescence deconvolution microscopy and image analysis

Images of cells on coverslips were acquired on a Delta Vision RT (Applied Precision, Image Solutions, UK) restoration microscope using a ×60 objective lens and appropriate wavelength filters. The images were collected using a Coolsnap HQ (Photometrics) camera with a Z optical spacing of 0.1 μm. Raw images were then deconvolved using Softworx software and displayed as maximum projections using NIH Image J ((W.S. Rasband, NIH Bethesda, USA; Wright Cell Imaging facility bundle: http://www.uhnres.utoronto.ca/facilities/wcif.htm).

Whole-cell patch-clamp electrophysiology

As described previously [21], COS-7 cells were transiently transfected with $Ca_v2.2$:β_{1b}: α_2/δ-1:mut3-GFP-pMT2 cDNA in a 3:1:1:0.2 mass ratio and current recordings made 48 h post-transfection. Where $\alpha_2\delta$-1 or mut-3 GFP was omitted, empty pcDNA3.1 vector was substituted to maintain the equivalent mass of DNA. Electrophysiological recordings of barium currents were made from green fluorescent COS-7 cells, using the whole-cell configuration of the patch clamp technique and the following solutions [71]. The internal solution contained (mM): caesium aspartate 140.0; EGTA 5.0; $MgCl_2$ 2.0; $CaCl_2$ 0.1; Hepes 20.0; K_2ATP 1.0; adjusted to pH 7.2 with CsOH and 310 mosm.l^{-1} with sucrose. The external solution contained (mM): TEABr

160.0; $MgCl_2$ 1.0; KCl 5.0; $NaHCO_3$ 1.0; Hepes 10.0; glucose 4.0; $BaCl_2$ 10; adjusted to pH 7.4 with Tris-base and to 320 mosm l^{-1} with sucrose. All experiments were performed at room temperature (20–22°C). An Axopatch 200B amplifier (Molecular Devices, Palo Alto, CA, USA) was used for recordings which were filtered at 2 Hz and digitised at 2–44 kHz using a Digidata 1440A A/D converter (Molecular Devices). Standard current-voltage protocols involved 150 ms sweeps from a holding potential, V_h of −80 mV to command voltages of −30 to +65 mV in 5 mV steps. Current density-voltage (*I-V*) relationships for each cell were fitted with a Boltzmann function:

$$I = (g(V - V_{rev}))/(1 + \exp(-(V - V_{50})/k)),$$

Where, V_{rev} is the reversal potential, V_{50} is the voltage for half maximal activation of current, g is the conductance, and k is the slope factor.

Data acquisition and analysis was performed using pCLAMP software (version 10, Molecular Devices) and Origin (version 7.0, Microcal, Northampton, MA, USA).

Data analysis

All data are presented as the mean ± standard error of the mean (S.E.M) for *n* trials. Statistical analysis was carried out by Student's t-test or ANOVA (one-way with Student-Newman-Keuls (SNK) *post hoc* correction), as appropriate, using 95% confidence limits (SigmaStat software, Jandel Scientific). Contour mapping was performed using Origin V.8 (OriginLab Corp., MA) on images converted from TIFF format to 2D matrices using the TIFFDump algorithm written by J.S Wadia [72]. Particle analysis was performed on thresholded images using NIH Image J.

Supporting Information

Figure S1 Effect of the GFP-tag on the biophysical properties of $Ca_v2.2/\beta_{1b}$ channels co-expressed with PIN-$\alpha_2\delta$ and PIN-$\alpha_2\delta$-PIN_{TMI}. *(A)* Average current density-voltage (*I-V*) plots for $Ca_v2.2/\beta_{1b}$ currents co-expressed with PIN-$\alpha_2\delta$ (open circle) versus PIN(deGFP)-$\alpha_2\delta$ (closed circle). *(B)* Average I-V plots for $Ca_v2.2/\beta_{1b}$ currents co-expressed with PIN-$\alpha_2\delta$-PIN_{TMI} (open circle) versus PIN(deGFP)-$\alpha_2\delta$-PIN_{TMI} (closed circle). Continuous lines indicate Boltzmann fits to *I-V* plot using the function described in the Methods. Panels *C*, *D*, show representative peak current traces for PIN-$\alpha_2\delta$ versus PIN(-deGFP)-$\alpha_2\delta$ (red) and PIN-$\alpha_2\delta$-PIN_{TMI} versus PIN(deGFP)-$\alpha_2\delta$-PIN_{TMI} (red), respectively. Histograms of the time constants of activation (τ_{act}) and inactivation (τ_{inact}) at peak current density for PIN(deGFP)-$\alpha_2\delta$-deGFP versus PIN-$\alpha_2\delta$ *(E)* and PIN(deGFP)-$\alpha_2\delta$-PIN_{TMI} versus PIN-$\alpha_2\delta$-PIN_{TMI}-deGFP *(F)*, where GFP-tagged (cross-hatched) and deGFP (red). τ_{act} and τ_{inact} were fitted with a single exponential function. Asterisks denote statistically significant differences (Student's t-test; ** = $P<0.01$; *** = $P<0.001$). Currents were evoked using 150 ms depolarising steps in 5 mV intervals (−30 to +65 mV), from a holding potential, V_h, −80 mV. Data are shown as the mean ± S.E.M. (TIF)

Figure S2 Particle analysis of PIN-$\alpha_2\delta$ cell surface clustering in the presence and absence of PI-PLC cell pre-treatment. A. Effect of PI-PLC on the size distribution of PIN-$\alpha_2\delta$ particles. Inset: data re-plotted using log scale. To facilitate overlay of images from separate cells, the number of particles Np_i, of given area (Ap_i, (abscissa) in pixel^2) is expressed as a percentage of the total (N_t where $N_t = \Sigma\ N_{Ai}$). Note overlap in data, irrespective of pre-treatment with PI-PLC. **B.** Distribution of fractional coverage represented by PIN-$\alpha_2\delta$ particles. Inset: data re-plotted using expanded scale. Here and elsewhere [21], we define fractional coverage as the % of the total particulate area (C_t) within a region of interest (ROI), (not the area of the ROI) accounted for by particles of area Ap_i (i.e. $Np_i.Ap_i/C_t$, where $C_t = \sum_{i=1}^{i=Ap'} Np_i.Ap_i$ and Ap' is the area of the largest particle in the data set). Using this representation it is possible to discriminate cases where coverage of the total particle area arises from many small particles or a lesser number of larger particles. For example, in the simple situation where there are 4 particles each of size 10 pixel^2 and 1 particle of size 60 pixel^2, then $C_t = 100$, then for the smaller particles $Np_i/N_t = 0.8$ and the fractional coverage = 0.4, for the larger particle $Np_i/N_t = 0.2$ and fractional coverage = 0.6. In contrast, if the same total particulate area is comprised of 60 particles each of size 1 pixel^2 and 4 particles each of size 10 pixel^2, then $Np_i/N_t = 0.94$ and the fractional coverage = 0.6, for the larger particles $Np_i/N_t = 0.06$ and fractional coverage = 0.4). Note overlap of data, irrespective of pre-treatment with PI-PLC. Particle analysis was performed with Image J, using the adaptive thresholding plug-in, with thresholded images checked visually for accuracy. All data were extracted from 3 images from separate experiments. **C.** and **D.** Computer modelling of the effects of particle re-distribution on fractional coverage Fractional coverage graphs (D) were determined for the three particle size distributions shown in C. Note marked, and well-defined effect of particle re-distribution. For simplicity, the distribution curves in C were generated using equations based on a binomial distribution with terms p^4 (black), $6p^2q^2$ (red) and q^4 (blue), (where q = 1-p), respectively. In each case, the number of particles N_t was adjusted to give an identical total particulate area, $C_t = 1\times10^5$ pixel^2 ((N_t = pixel^2, black, red and blue curves, respectively). **E.** and **F.** Computer modelling of the effects of a reduction in particle area. In these simulations the number of particles was held constant ($Nt = 10^4$), but the area of each decreased by 50% to mimic a 'stripping' effect such as that which might be seen with PI-PLC. Curves in E. were generated as in C., for the p^4 binomial distribution. From comparisons of the size distribution and fractional coverage determined experimentally (A, B) and predicted from simulations (C–F), there is no evidence that PI-PLC pre-treatment has any effect on PIN-$\alpha_2\delta$ particle properties. (TIF)

Figure S3 Comparative analysis of GPI-anchoring motifs. A. Comparison of carboxy-terminal sequences of known GPI-anchored proteins and rat $\alpha_2\delta$-1,2,3 & 4 showing the ω site(s) (red lettering) and hydrophobic regions (grey boxes) of the GPI-anchoring motifs. All dataset examples (i.e. non-$\alpha_2\delta$) correspond to proteins where the ω site has been verified, experimentally. (References: P21589: Misumi, Y. et al. (1990) Eur. J. Biochem. 191:563–569; P22748: Okuyama, T. et al. (1995) Arch. Biochem. Biophys. 320:315–322; P08174: Moran, P. et al. (1991) J. Biol. Chem. 266:1250–1257; P04058: Mehlert, A., et al. (1993) Biochem. J. 296:473–479; P15328 & P14207: Yan, W. and Ratnam, M. (1995) Biochemistry 34:14594–14600; P01831: Williams, A.F. and Gagnon, J. (1982) Science 216:696–703; P16444: Adachi, H. et al. (1990) J. Biol. Chem. 265:15341–15345; P31358: Xia, M.Q. et al. (1993) Biochem. J. 293:633–640; P04273: Stahl, N. et al. (1990) Biochemistry 29:8879–8884; P13987: Sugita, Y. et al. (1993) J. Biochem. 114:473–477; P05187: Micanovic, R. et al. (1990) Proc. Natl. Acad. Sci. U.S.A. 87:157–161; P14384: Tan, F. et al. (2003) Biochem. J. 370:567–578; XP_001352170.1: Hall, N. et al. (2002) Nature 419:527–531). The $\alpha_2\delta$-1-3 ω sites have been tested, experimentally (Davies et al., 2010, Robinson et al., 2010 above), while that for $\alpha_2\delta$-4 is inferred based on sequence homology to $\alpha_2\delta$-3. B. Left panel: Potential for

GPI-modification for dataset and $\alpha_2\delta$ proteins shown in A inferred using Big-Pi predictor software (http://expasy.org/tools/). Proteins with positive or negative GPI modification potential are shown in blue and red, respectively. Asterisks denote proteins where the ω site differs from that inferred. Right panel detailed sequence comparison of inferred (red lettering) and predicted (asterisks) ω sites. In most cases the inferred ω site is very close (<2 residues) to that found experimentally. C. Analysis of potential upstream GPI-anchoring motifs in the delta subunit of WT $\alpha_2\delta$-1 (or PIN-$\alpha_2\delta$)(blue) and PIN-$\alpha_2\delta$-PIN_{TMI} (red). Here, the GPI anchoring potential was determined (using Big-Pi [29]) as a function of successive truncation (1 residue at a time) of the carboxy terminus. Note: based on the length of the GPI-anchoring motif, any ω site is predicted to lie 20–30 residues upstream of the position of the indicated carboxy-terminal residue (abscissa). For simplification, the carboxy-terminal sequences have been re-numbered starting at residue 922 in WT $\alpha_2\delta$-1 as shown in the corresponding sequences (i. and ii. right panel). For PIN-$\alpha_2\delta$, the reported GPI-anchoring motif is shown in blue lettering. For PIN-$\alpha_2\delta$-PIN_{TMI} green lettering denotes residues derived from PIN-G. In i. and ii., the grey boxes denote hydrophobic regions. With the exception of sequences near the junction of the α_2 and δ delta subunits, all regions have a much lower GPI-modification potential than the WT $\alpha_2\delta$ C-terminus suggesting the likely absence of additional upstream GPI-anchoring motifs unmasked by proteolytic cleavage. Note, the low GPI-modification potential of both the non-truncated PIN-$\alpha_2\delta$ and PIN-$\alpha_2\delta$-PIN_{TMI}.
(TIF)

Table S1 Biophysical properties of $Ca_v2.2/\beta_{1b}$ channels co-expressed with WT $\alpha_2\delta$-1, PIN-$\alpha_2\delta$, PIN-$\alpha_2\delta$-PIN_{TMI} and PIN-δ. I_{max} is the maximum peak current density. Individual current density-voltage plots were fitted with a Boltzmann function:

$$I = (g(V - V_{rev}))/(1 + \exp(-(V - V_{50,act})/k)),$$

where V_{rev} is the reversal potential, $V_{50,act}$ is the voltage for half maximal activation of current, g is the conductance, and k is the slope factor. Statistical analysis used Students unpaired t-test. Asterisks denote statistically significant differences from (−)$\alpha_2\delta$-1, as follows: * = $P<0.05$, *** = $P<0.001$. n is the number of cells tested per treatment.
(DOC)

Acknowledgments

We would like to thank Dr. Felix Elortza (CICbioGUNE, Derio, Spain) for advice regarding proteomics and predictive analysis of GPI-anchored proteins.

Author Contributions

Conceived and designed the experiments: OTJ EMF PR. Performed the experiments: PR LS SE RS. Analyzed the data: PR OTJ EMF LS. Contributed reagents/materials/analysis tools: OTJ EMF. Wrote the paper: OTJ EMF.

References

1. Catterall WA, Perez-Reyes E, Snutch TP, Striessnig J (2005) International Union of Pharmacology XLVIII Nomenclature and structure-function relationships of voltage-gated calcium channels. Pharmacol Rev 57: 411–425.
2. Perret D, Luo ZD (2009) Targeting voltage-gated calcium channels for neuropathic pain management. Neurotherapeutics 6: 679–692.
3. Splawski I, Timothy KW, Decher N, Kumar P, Sachse FB, et al. (2005) Severe arrhythmia disorder caused by cardiac L-type calcium channel mutations. Proc Natl Acad Sci USA 102: 8089–8096.
4. Dai S, Hall DD, Hell JW (2009) Supramolecular assemblies and localized regulation of voltage-gated ion channels. Physiol Rev 89: 411–452.
5. Ertel EA, Campbell KP, Harpold MM, Hofmann F, Mori Y, et al. (2000) Nomenclature of voltage-gated calcium channels. Neuron 25: 533–535.
6. Canti C, Nieto-Rostro M, Foucault I, Heblich F, Wratten J, et al. (2005) The metal-ion-dependent adhesion site in the Von Willebrand factor-A domain of α2δ subunits is key to trafficking voltage-gated Ca^{2+} channels. Proc Natl Acad Sci USA 102: 11230–11235.
7. Davies A, Hendrich J, Van Minh AT, Wratten J, Douglas L, et al. (2007) Functional biology of the $\alpha_2\delta$ subunits of voltage-gated calcium channels. Trends Pharmacol Sci 28: 220–280.
8. Elliott EM, Malouf AT, Catterall WA (1995) Role of calcium channel subtypes in calcium transients in hippocampal CA3 neurons. J Neurosci 15: 6433–6444.
9. Pani B, Singh BB (2009) Lipid rafts/caveolae as microdomains of calcium signalling. Cell Calcium 45: 625–633.
10. Müller CS, Haupt A, Bildl W, Schindler J, Knaus HG, et al. (2010) Quantitative proteomics of the Cav2 channel nano-environments in the mammalian brain. Proc Natl Acad Sci U S A 107: 14950–14957.
11. Striessnig J, Koschak A (2008) Exploring the function and pharmacotherapeutic potential of voltage-gated Ca^{2+} channels with gene knockout models. Channels (Austin) 2: 233–251.
12. Vacher H, Mohapatra DP, Trimmer JS (2008) Localization and targeting of voltage-dependent ion channels in mammalian central neurons. Physiol Rev 88: 1407–1447.
13. Dart C (2010) Lipid microdomains and the regulation of ion channel function. J Physiol 588: 3169–3178.
14. Lingwood D, Simons K (2010) Lipid rafts as a membrane-organizing principle. Science 327: 46–50.
15. Foster LJ, De Hoog CL, Mann M (2003) Unbiased quantitative proteomics of lipid rafts reveals high specificity for signaling factors. Proc Natl Acad Sci U S A 100: 5813–5818.
16. Toselli M, Biella G, Taglietti V, Cazzaniga E, Parenti M (2005) Caveolin-1 expression and membrane cholesterol content modulate N-type calcium channel activity in NG108-15 cells. Biophys J 89: 2443–2457.
17. Balijepalli RC, Foell JD, Hall DD, Hell JW, Kamp TJ (2006) Localization of cardiac L-type Ca^{2+} channels to a caveolar macromolecular signaling complex is required for β_2-adrenergic regulation. Proc Natl Acad Sci USA 103: 7500–7505.
18. Davies A, Douglas L, Hendrich J, Wratten J, Van Minh AT, et al. (2006) The calcium channel α2δ-2 subunit partitions with $Ca_v2.1$ into lipid rafts in cerebellum: Implications for localization and function. J Neurosci 26: 8748–8757.
19. Xia F, Leung YM, Gaisano G, Gao X, Chen Y, et al. (2007) Targeting of voltage-gated K^+ and Ca^{2+} channels and soluble N-ethylmaleimide-sensitive factor attachment protein receptor proteins to cholesterol-rich lipid rafts in pancreatic alpha-cells: effects on glucagon stimulus-secretion coupling. Endocrinology 148: 2157–2167.
20. Davies A, Kadurin I, Alvarez-Laviada A, Douglas L, Nieto-Rostro M, et al. (2010) The $\alpha_2\delta$ subunits of voltage-gated calcium channels form GPI-anchored proteins, a posttranslational modification essential for function. Proc Natl Acad Sci U S A 107: 1654–1659.
21. Robinson P, Etheridge S, Song L, Armenise P, Jones OT, et al. (2010) Formation of N-type (Cav2.2) voltage-gated calcium channel membrane microdomains: Lipid raft association and clustering. Cell Calcium 48: 183–194.
22. Jacobo SM, Guerra ML, Jarrard RE, Przybyla JA, Liu G, et al. (2009) The intracellular II-III loops of $Ca_v1.2$ and $Ca_v1.3$ uncouple L-type voltage-gated Ca^{2+} channels from glucagon-like peptide-1 potentiation of insulin secretion in INS-1 cells via displacement from lipid rafts. J Pharmacol Exp Ther 330: 283–293.
23. De Jongh KS, Warner C, Catterall WA (1990) Subunits of purified calcium channels. J Biol Chem 265: 14738–14741.
24. Wiser O, Trus M, Tobi D, Halevi S, Giladi E, et al. (1996) The alpha 2/delta subunit of voltage-sensitive Ca^{2+} channels is a single transmembrane extracellular protein which is involved in regulated secretion. FEBS Lett 379: 15–20.
25. Jay SD, Sharp AH, Kahl SD, Vedvick TS, Harpold MM, et al. (1991) Structural characterization of the dihydropyridine-sensitive calcium channel α_2-subunit and the associated δ peptides. J Biol Chem 266: 3287–3293.
26. Whittaker CA, Hynes RO (2002) Distribution and evolution of von Willebrand/Integrin A domains: Widely dispersed domains with roles in cell adhesion and elsewhere. Molec Biol Cell 13: 3369–3387.
27. Eroglu C, Allen NJ, Susman MW, O'Rourke NA, Park CY, et al. (2009) Gabapentin receptor $\alpha_2\delta$-1 is a neuronal Thrombospondin receptor responsible for excitatory CNS synaptogenesis. Cell 139: 380–392.
28. Gurnett CA, De Waard M, Campbell KP (1996) Dual function of the voltage-dependent Ca^{2+} channel $\alpha_2\delta$ subunit in current stimulation and subunit interaction. Neuron 16: 431–440.

29. Felix R, Gurnett CA, DeWaard M, Campbell KP (1997) Dissection of functional domains of the voltage-dependent Ca^{2+} channel $\alpha_2\delta$ subunit. J Neurosci 17: 6884–6891.
30. Eisenhaber B, Bork P, Eisenhaber F (1999) Prediction of potential GPI-modification sites in proprotein sequences. J Mol Biol 292: 741–758.
31. Zacks MA, Garg N (2006) Recent developments in the molecular, biochemical and functional characterization of GPI8 and the GPI-anchoring mechanism. Mol Membr Biol 23: 209–225.
32. Paulick MG, Bertozzi CR (2008) The glycosylphosphatidylinositol anchor: a complex membrane-anchoring structure for proteins. Biochemistry 47: 6991–7000.
33. Brown DA, Rose JK (1992) Sorting of GPI-anchored proteins to glycolipid-enriched membrane subdomains during transport to the apical cell surface. Cell 68: 533–544.
34. Levental I, Grzybek M, Simons K (2010) Greasing their way: lipid modifications determine protein association with membrane rafts. Biochemistry 49: 6305–6316.
35. Bauer CS, Tran-Van-Minh A, Kadurin I, Dolphin AC (2010) A new look at calcium channel $\alpha_2\delta$ subunits. Curr Opin Neurobiol 20: 563–571.
36. Gurnett CA, Felix R, Campbell KP (1997) Extracellular interaction of the voltage-dependent Ca^{2+} channel $\alpha_2\delta$ and α_1 subunits. J Biol Chem 272: 18508–18512.
37. Quinn PJ (2010) A lipid matrix model of membrane raft structure. Prog Lipid Res 49: 390–406.
38. Lundbaek JA, Andersen OS, Werge T, Nielsen C (2003) Cholesterol-induced protein sorting: an analysis of energetic feasibility. Biophys J 84: 2080–2089.
39. Baumgart T, Hammond AT, Sengupta P, Hess ST, Holowka DA, et al. (2007) Large-scale fluid/fluid phase separation of proteins and lipids in giant plasma membrane vesicles. Proc Natl Acad Sci U S A 104: 3165–3170.
40. Chichili GR, Rodgers W (2007) Clustering of membrane raft proteins by the actin cytoskeleton. J Biol Chem 282: 36682–36691.
41. Goswami D, Gowrishankar K, Bilgrami S, Ghosh S, Raghupathy R, et al. (2008) Nanoclusters of GPI-anchored proteins are formed by cortical actin-driven activity. Cell 135: 1085–1097.
42. Chen Y, Veracini L, Benistant C, Jacobson K (2009) The transmembrane protein CBP plays a role in transiently anchoring small clusters of Thy-1, a GPI-anchored protein, to the cytoskeleton. J Cell Sci 122: 3966–3972.
43. Douglass AD, Vale RD (2005) Single-molecule microscopy reveals plasma membrane microdomains created by protein-protein networks that exclude or trap signaling molecules in T cells. Cell 121: 937–950.
44. Stetzkowski-Marden F, Gaus K, Recouvreur M, Cartaud A, Cartaud J (2006) Agrin elicits membrane lipid condensation at sites of acetylcholine receptor clusters in C2C12 myotubes. J Lipid Res 47: 2121–2133.
45. Ge M, Gidwani A, Brown HA, Holowka D, Baird B, et al. (2003) Ordered and disordered phases coexist in plasma membrane vesicles of RBL-2H3 mast cells. An ESR study. Biophys J 85: 1278–1288.
46. Kaiser HJ, Lingwood D, Levental I, Sampaio JL, Kalvodova L, et al. (2009) Order of lipid phases in model and plasma membranes. Proc Natl Acad Sci U S A 106: 16645–16650.
47. Nikolaus J, Scolari S, Bayraktarov E, Jungnick N, Engel S, et al. (2010) Hemagglutinin of influenza virus partitions into the nonraft domain of model membranes. Biophys J 99: 489–498.
48. Incardona JP, Rosenberry TL (1996) Replacement of the glycoinositol phospholipid anchor of Drosophila acetylcholinesterase with a transmembrane domain does not alter sorting in neurons and epithelia but results in behavioral defects. Mol Biol Cell 7: 613–630.
49. Wang J, Maziarz K, Ratnam M (1999) Recognition of the carboxyl-terminal signal for GPI modification requires translocation of its hydrophobic domain across the ER membrane. J Mol Biol 286: 1303–1310.
50. Verghese GM, Gutknecht MF, Caughey GH (2006) Prostasin regulates epithelial monolayer function: cell-specific Gpld1-mediated secretion and functional role for GPI anchor. Am J Physiol Cell Physiol 291: C1258–C1270.
51. McKeown L, Robinson P, Greenwood SM, Hu W, Jones OT (2006) PIN-G - a novel reporter for imaging and defining the effects of trafficking signals in membrane proteins. BMC Biotechnol 6: 15.
52. Poisson G, Chauve C, Chen X, Bergeron A (2007) FragAnchor a large scale all Eukaryota predictor of Glycosylphosphatidylinositol-anchor in protein sequences by qualitative scoring. Genomics, Proteomics & Bioinformatics 5: 121–130.
53. Pierleoni A, Martelli PL, Casadio R (2008) PredGPI: a GPI-anchor predictor. BMC Bioinformatics 9: 392.
54. Nichols BJ, Kenworthy AK, Polishchuk RS, Lodge R, Roberts TH, et al. (2001) Rapid cycling of lipid raft markers between the cell surface and Golgi complex. J Cell Biol 153: 529–541.
55. Sandoval A, Oviedo N, Andrade A, Felix R (2004) Glycosylation of asparagines 136 and 184 is necessary for the $\alpha_2\delta$ subunit-mediated regulation of voltage-gated Ca^{2+} channels. FEBS Lett 576: 21–26.
56. Schroeder R, London E, Brown D (1994) Interactions between saturated acyl chains confer detergent resistance on lipids and glycosylphosphatidylinositol (GPI)-anchored proteins: GPI-anchored proteins in liposomes and cells show similar behavior. Proc Natl Acad Sci U S A 91: 12130–12134.
57. Sengupta P, Hammond A, Holowka D, Baird B (2008) Structural determinants for partitioning of lipids and proteins between coexisting fluid phases in giant plasma membrane vesicles. Biochim Biophys Acta 1778: 20–32.
58. Ferguson MA, Low MG, Cross GA (1985) Glycosyl-sn-1,2-dimyristylphosphatidylinositol is covalently linked to Trypanosoma brucei variant surface glycoprotein. J Biol Chem 260: 14547–14555.
59. Elortza F, Nühse TS, Foster LJ, Stensballe A, Peck SC, et al. (2003) Proteomic analysis of glycosylphosphatidylinositol-anchored membrane proteins. Mol Cell Proteomics 2: 1261–1270.
60. Mayor S, Maxfield FR (1995) Insolubility and redistribution of GPI-anchored proteins at the cell surface after detergent treatment. Mol Biol Cell 6: 929–944.
61. Parton RG, Hanzal-Bayer M, Hancock JF (2006) Biogenesis of caveolae: a structural model for caveolin-induced domain formation. J Cell Sci 119: 787–796.
62. Browman DT, Hoegg MB, Robbins SM (2007) The SPFH domain-containing proteins: more than lipid raft markers. Trends Cell Biol 17: 394–402.
63. Bernstein GM, Jones OT (2006) Kinetics of internalization and degradation of N-type voltage-gated calcium channels: Role of the $\alpha_2\delta$ subunit. Cell Calcium 41: 27–40.
64. Su B, Bothwell AL (1989) Biosynthesis of a phosphatidylinositol-glycan-linked membrane protein: signals for posttranslational processing of the Ly-6E antigen. Mol Cell Biol 9: 3369–3376.
65. Watanabe K, Nagaoka T, Strizzi L, Mancino M, Gonzales M, et al. (2008) Characterization of the glycosylphosphatidylinositol-anchor signal sequence of human Cryptic with a hydrophilic extension. Biochimica et Biophysica Acta 1778: 2671–2681.
66. Woodman SE, Park DS, Cohen AW, Cheung MW-C, Chandra M, et al. (2002) Caveolin-3 Knock-out Mice Develop a Progressive Cardiomyopathy and Show hyperactivation of the p42/44 MAPK Cascade. J Biol Chem 277: 38988–38997.
67. Ibarguren M, Lopez DJ, Montes LR, Sot J, Vasil AI, et al. (2011) Imaging the early stages of phospholipase C/sphingomyelinase activity on vesicles containing coexisting ordered-disordered and gel-fluid domains. J Lipid Res 52: 635–645.
68. Stuermer CA (2011) Microdomain-forming proteins and the role of thereggies/flotillins during axon regeneration in zebrafish. Biochim Biophys Acta 1812: 415–422.
69. Kusumi A, Suzuki K (2005) Toward understanding the dynamics of membrane-raft-based molecular interactions. Biochim Biophys Acta 1746: 234–251.
70. Geiser M, Cèbe R, Drewello D, Schmitz R (2001) Integration of PCR fragments at any specific site within cloning vectors without the use of restriction enzymes and DNA ligase. Biotechniques 31: 88–90, 92.
71. Hamill OP, Marty A, Neher E, Sakmann B, Sigworth FJ (1981) Improved patch-clamp techniques for high-resolution current recording from cells and cell-free membrane patches. Pflugers Arch 391: 85–100.
72. Bernstein GM, Mendonca A, Wadia J, Burnham WM, Jones OT (1999) Kindling induces a long-term enhancement in the density of N-type calcium channels in the rat hippocampus. Neuroscience 94: 1083–1109.